

Electron-phonon scattering in topological insulators

Sébastien Giraud and Reinhold Egger

Institut für Theoretische Physik, Heinrich-Heine-Universität, D-40225 Düsseldorf, Germany

(Dated: January 13, 2013)

We formulate and apply a theory of electron-phonon interactions for the surface state of a strong topological insulator. Phonons are modelled using an isotropic elastic continuum theory with stress-free boundary conditions and interact with the Dirac surface fermions via the deformation potential. We discuss the temperature dependence of the quasi-particle lifetime in photoemission and of the surface resistivity.

PACS numbers: 73.20.-r, 63.20.kd, 72.10.Di

Introduction.— One of the presently most active areas in physics is concerned with strong topological insulator (TI) materials [1, 2]. In these systems strong spin-orbit couplings cause band inversion and a nontrivial topology of the map from momentum to Hilbert space [3, 4]. In a TI, as long as time-reversal invariance remains unbroken, an odd number of massless surface Dirac fermion modes is guaranteed despite of the presence of a bulk gap Δ_b . The existence of metallic two-dimensional (2D) Dirac surface states has been convincingly established using angle-resolved photoemission spectroscopy (ARPES) in bismuth selenides [1, 5]. Typical reference materials are Bi_2Te_3 or Bi_2Se_3 , where $\Delta_b \simeq 0.3$ eV allows to observe these phenomena even at room temperature, but other material classes have also been predicted to possess a TI phase [1]. Attempts to observe electronic transport signatures of the surface state were only partially successful [6–8] since surface effects are easily masked by defect-induced residual bulk charge carriers. Anticipating progress in achieving better purity, it is important to understand what intrinsically limits the surface conductivity and the integrity of surface quasi-particles. Noting that the large and anisotropic static dielectric constant ($\epsilon \approx 50$ to 200 [9]) implies a drastic reduction of direct Coulomb forces or charged impurity potentials, we here analyze consequences of the *electron-phonon coupling* on the TI surface state.

We focus on long-wavelength acoustic phonons which dominate the physics at low energy scales. Previous work on the thermoelectric properties of Bi_2Te_3 has demonstrated that despite of the quintuple-layer crystal structure, bulk acoustic phonons are reasonably well described as isotropic elastic continuum [10, 11], where the two Lamé parameters of the theory determine the longitudinal and transverse sound velocities, $c_l \simeq 2800$ m/s and $c_t \simeq 1600$ m/s, respectively. Low-temperature electronic transport is then limited by the deformation potential coupling to acoustic phonons, since piezoelectric couplings are suppressed by inversion symmetry [11]. TI experiments have so far only addressed the coupling to optical phonons [9, 12], cf. also studies for Bi surfaces [13]. However, massless 2D Dirac fermions are realized in graphene monolayers as well, where both theory [14, 15] and experiment [16] have reported consistent results for the temperature (T) dependence of the resistivity (ρ):

for $T \ll T_{\text{BG}}$ (with the Bloch-Grüneisen temperature $T_{\text{BG}} \equiv 2\hbar k_F c_s / k_B$, Fermi momentum k_F , and sound velocity c_s), a $\rho \sim T^4$ scaling is found, while $\rho \sim T$ for $T \gg T_{\text{BG}}$. Note that for a 2D electron gas with parabolic dispersion and dominant deformation potential coupling, one expects $\rho \sim T^7$ for $T \ll T_{\text{BG}}$ [17]. Below, we shall discuss the $\rho(T)$ dependence of the TI surface state due to the coupling to acoustic phonons in detail. In addition, phonons are expected to cause quasi-particle decay. This implies, e.g., a finite ARPES linewidth [18, 19], where an anomalous behavior was observed in Bi_2Se_3 [20].

In this paper, we formulate and study an analytically tractable effective low-energy theory for the TI surface state coupled to acoustic phonons. The phonon modes are obtained from isotropic elastic continuum theory in a half-space with stress-free boundary conditions [21, 22]. Their coupling to the surface fermions is predominantly via the deformation potential [23]. For concrete numbers, we use published [10, 11, 24] values for Bi_2Te_3 . We compute the quasi-particle decay rate Γ and find $\Gamma \sim T$ at high temperatures. This prediction should be observable by ARPES. Phonons also affect the surface resistivity and yield a characteristic T -dependent contribution to ρ . Our theory is flexible enough to allow for the use of microscopically derived phonon modes and coupling matrix elements, e.g., resulting from (future) numerical force-constant calculations.

Model.— We consider energies below the TI bulk gap where only surface electronic states are relevant. For the half-space $z > 0$, the surface-state wave function $\chi(z)$ follows from the low-energy band structure with Dirichlet boundary conditions at $z = 0$ [25],

$$\chi(z) = \mathcal{N}(e^{-\eta_- z} - e^{-\eta_+ z}), \quad \eta_{\pm} = \frac{B_0 \pm \sqrt{B_0^2 + 4M_0 M_1}}{2M_1} \quad (1)$$

with normalization \mathcal{N} and material parameters (B_0, M_0, M_1) specified in Ref. [24]. Since $M_0 M_1 < 0$ and $B_0/M_1 > 0$, we have $\text{Re}(\eta_{\pm}) > 0$ and the state (1) decays exponentially. One arrives at a massless 2D Dirac Hamiltonian (we set $\hbar = 1$) [1],

$$H_e = \sum_{\mathbf{k}, s=\pm} \epsilon_{\mathbf{k}s} c_{\mathbf{k}s}^\dagger c_{\mathbf{k}s}, \quad \epsilon_{\mathbf{k}s} = s v_F |\mathbf{k}| - \mu, \quad (2)$$

with the Fermi velocity $v_F \simeq 4.36 \times 10^5$ m/s and the

chemical potential μ defining $k_F = |\mu|/v_F$. A helical eigenstate with helicity $s = \pm$ has its spin structure tied to the surface momentum $\mathbf{k} = (k_x, k_y)$. Helical fermions, $c_{\mathbf{k}} = (c_{\mathbf{k}+}, c_{\mathbf{k}-})^T$, are connected to the usual spinful operators, $d_{\mathbf{k}} = (d_{\mathbf{k}\uparrow}, d_{\mathbf{k}\downarrow})^T$, by a unitary transformation,

$$c_{\mathbf{k}} = U_{\mathbf{k}} d_{\mathbf{k}}, \quad U_{\mathbf{k}} = \frac{1}{\sqrt{2}} \begin{pmatrix} e^{i\theta_{\mathbf{k}}/2} & ie^{-i\theta_{\mathbf{k}}/2} \\ e^{i\theta_{\mathbf{k}}/2} & -ie^{-i\theta_{\mathbf{k}}/2} \end{pmatrix}, \quad (3)$$

where $\tan \theta_{\mathbf{k}} = k_y/k_x$.

In order to describe noninteracting acoustic phonons we employ isotropic elastic continuum theory with stress-free boundary conditions at $z = 0$. We briefly summarize the resulting eigenmodes [21, 22] before turning to the electron-phonon coupling. Following the notation in Ref. [22] we label the modes by the quantum numbers $\Lambda = (\mathbf{q}, \Omega, \lambda)$, with surface momentum $\mathbf{q} = (q_x, q_y)$, frequency $\Omega > 0$, and mode type $\lambda \in (H, T, L, R)$ explained below. In this non-standard but very convenient notation, the frequency $\Omega = \Omega_{\Lambda}$ is not specified in terms of \mathbf{q} and λ but represents a free parameter. With $\mathbf{r} = (x, y)$ and surface area \mathcal{A} , the displacement field operator takes the form

$$\mathbf{U}(\mathbf{r}, z, t) = \sum_{\Lambda} \frac{1}{\sqrt{2\rho_M \mathcal{A} \Omega}} \mathbf{u}_{\Lambda}(z) e^{i(\mathbf{q} \cdot \mathbf{r} - \Omega t)} b_{\Lambda} + \text{h.c.}, \quad (4)$$

where b_{Λ} is a bosonic annihilation operator and $\rho_M \simeq 7860 \text{ kg/m}^3$ [10]. The noninteracting phonon Hamiltonian is $H_p = \sum_{\Lambda} \Omega_{\Lambda} (b_{\Lambda}^{\dagger} b_{\Lambda} + 1/2)$. The orthonormal eigenmodes $\mathbf{u}_{\Lambda}(z)$ describe linear combinations of $e^{\pm i k_{l,t} z}$ waves, where $k_{l,t} = \sqrt{(\Omega/c_{l,t})^2 - q^2}$. First, the horizontal shear mode, $\lambda = H$, with $\mathbf{u}_H \parallel \hat{e}_z \times \hat{e}_q$ (where $\hat{e}_q = \mathbf{q}/q$) decouples from all other modes and does not generate a deformation potential; hence it is not discussed further. The remaining modes are given by

$$\mathbf{u}(z) = \left(i q \phi_l - \frac{d\phi_t}{dz} \right) \hat{e}_q + \left(\frac{d\phi_l}{dz} + i q \phi_t \right) \hat{e}_z, \quad (5)$$

$$\phi_{l,t} = \frac{1}{\sqrt{2\pi\Omega k_{l,t}}} (a_{l,t} e^{-i k_{l,t} z} + b_{l,t} e^{i k_{l,t} z}).$$

The incoming longitudinal mode, $\lambda = L$, with $a_l = 1$ and $a_t = 0$, exists for $\Omega > c_l q$ with real $k_{l,t} > 0$. The eigenstate $\phi_{l,t}^{(L)}$ has $b_l = -A$ and $b_t = B$, where

$$A = \frac{(q^2 - k_t^2)^2 - 4q^2 k_l k_t}{(q^2 - k_t^2)^2 + 4q^2 k_l k_t}, \quad B = \frac{4q(q^2 - k_t^2)\sqrt{k_l k_t}}{(q^2 - k_t^2)^2 + 4q^2 k_l k_t}.$$

The incoming transverse mode, $\lambda = T$, with $a_l = 0$ and $a_t = 1$, exists for $\Omega > c_t q$. The eigenstate $\phi_{l,t}^{(T)}$ has $b_l = -B$ and $b_t = -A$. (For $c_t q < \Omega < c_l q$, we have $k_l = i|k_l|$.) Finally, the energetically lowest solution is the Rayleigh surface wave, $\lambda = R$, where $a_l = a_t = 0$ and $k_{l,t} = i\kappa_{l,t} q$. Here the dispersion relation is linear, $\Omega = c_R q$ with surface velocity $c_R = \xi c_t$, i.e., Ω is not a free parameter in Λ anymore. Putting $\gamma = (c_t/c_l)^2$, we find

$$\xi = \left(\frac{8}{3} - \frac{4\sqrt{12\gamma - 2}}{3} \cos \left[\frac{1}{3} \cos^{-1} \left(\frac{17 - 45\gamma}{(12\gamma - 2)^{3/2}} \right) \right] \right)^{1/2}.$$

With $\kappa_l = \sqrt{1 - \gamma\xi^2}$ and $\kappa_t = \sqrt{1 - \xi^2}$, we obtain

$$\phi_l^{(R)} = \sqrt{\frac{C}{q}} e^{-\kappa_l q z}, \quad \phi_t^{(R)} = -\sqrt{\frac{C}{q}} \frac{2i\kappa_l}{1 + \kappa_t^2} e^{-\kappa_t q z},$$

$$C^{-1} = \kappa_l - \kappa_t + \frac{(\kappa_l - \kappa_t)^2}{2\kappa_l^2 \kappa_t}. \quad (6)$$

Using the above values for $c_{l,t}$ we find $\xi \simeq 0.92$, $\kappa_l \simeq 0.85$, $\kappa_t \simeq 0.39$ and $C \simeq 1.20$.

Electron-phonon coupling.— The deformation potential couples the local electron density to $\nabla \cdot \mathbf{U}(\mathbf{r}, z)$, with a coupling constant α . Ref. [11] gives the estimate $\alpha \approx 35 \text{ eV}$. This yields the second-quantized interaction Hamiltonian

$$H_{ep} = \frac{\alpha}{\sqrt{\mathcal{A}}} \sum_{\mathbf{q}\Omega\lambda} M_{\mathbf{q}\Omega}^{(\lambda)} b_{\mathbf{q}\Omega\lambda} \sum_{\mathbf{k}ss'} c_{\mathbf{k}+\mathbf{q},s}^{\dagger} X_{\mathbf{k}\mathbf{q},ss'} c_{\mathbf{k}s'} + \text{h.c.}, \quad (7)$$

where $U_{\mathbf{k}}$ in Eq. (3) defines the matrix $X_{\mathbf{k}\mathbf{q}} = U_{\mathbf{k}+\mathbf{q}} U_{\mathbf{k}}^{\dagger}$. For the Rayleigh mode, the sum over Ω should be omitted with the replacement $\Omega = c_R q$. With $\phi_l^{(\lambda)}$ specified in Eqs. (5) and (6), we obtain the \hat{e}_q -independent electron-phonon coupling matrix elements

$$M_{\mathbf{q}\Omega}^{(\lambda)} = -\frac{(\Omega/c_l)^2}{\sqrt{2\rho_M \Omega}} \int_0^{\infty} dz |\chi(z)|^2 \phi_l^{(\lambda)}(z), \quad (8)$$

with the electronic surface state χ in Eq. (1). For $q \ll \text{Re}(\eta_-)$, the overlap integral above reduces to $\phi_l^{(\lambda)}(z=0)$. In what follows, we discuss physical consequences obtained from the Hamiltonian $H = H_e + H_p + H_{ep}$. In the concrete examples below, the chemical potential is $\mu = v_F k_F = 0.05 \text{ eV}$, corresponding to the BG temperature $T_{\text{BG}} = 2k_F c_R / k_B = 3.9 \text{ K}$ and the Fermi temperature $T_F = 580 \text{ K}$.

Lifetime broadening.— We begin with the self-energy $\Sigma_s(\mathbf{k}, \omega)$ for a helical eigenstate $s = \pm$. Following standard arguments [18, 19], the main contribution is captured to lowest nontrivial order in H_{ep} . Noting that the “tadpole” diagram vanishes identically, the “rainbow” diagram [18] yields independent contributions from each mode λ ,

$$\Sigma_s^{(\lambda)}(\mathbf{k}, \omega) = \sum_{s', \nu=\pm} \alpha^2 \int_0^{\infty} d\Omega \int \frac{d^2 \mathbf{q}}{(2\pi)^2} \left| M_{\mathbf{q}\Omega}^{(\lambda)} X_{\mathbf{k}\mathbf{q},ss'} \right|^2$$

$$\times \frac{\nu [n_B(\nu\Omega) + n_F(\epsilon_{\mathbf{k}+\mathbf{q},s'})]}{\omega + i0^+ + \nu\Omega - \epsilon_{\mathbf{k}+\mathbf{q},s'}}, \quad (9)$$

where n_B (n_F) is the Bose (Fermi) function. For the R mode, the q -integral has to include the additional factor $\delta(\Omega - c_R q)$, while for $\lambda = L, T$, we have the respective constraint $q < \Omega/c_{l,t}$. The decay rate $\Gamma^{(\lambda)} = -2 \text{Im} \Sigma^{(\lambda)}$ describing lifetime broadening is then given by

$$\Gamma_s^{(\lambda)}(\mathbf{k}, \omega) = \sum_{\nu=\pm} \alpha^2 \int_0^{\infty} d\Omega F_{\mathbf{k}s,\omega}^{(\lambda\nu)}(\Omega)$$

$$\times [n_B(\Omega) + n_F(\Omega + \nu\omega)]. \quad (10)$$

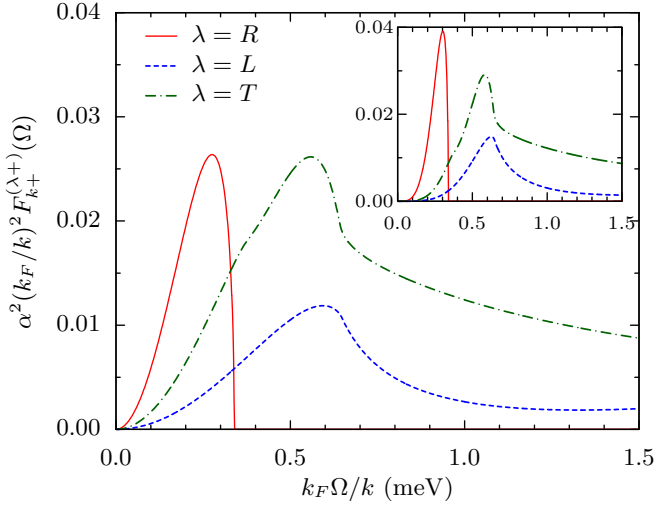


FIG. 1. (Color online) Low-frequency behavior of the Eliashberg functions $F_{k+}^{(\lambda+)}(\Omega)$ for the three relevant acoustic phonon modes ($k = 0.1k_F$). In the rescaled units used here, the functions are approximately k -independent. Inset: Same for the “transport” Eliashberg function \mathcal{F} (see main text).

Here the Eliashberg function [18] is defined as

$$F_{\mathbf{k}s,\omega}^{(\lambda\pm)}(\Omega) = \sum_{s'} \int \frac{d^2\mathbf{q}}{2\pi} \left| M_{q\Omega}^{(\lambda)} X_{\mathbf{k}\mathbf{q},ss'} \right|^2 \delta(\omega \pm \Omega - \epsilon_{\mathbf{k}+\mathbf{q},s'}) \quad (11)$$

which represents a phonon density of states weighted by the coupling matrix elements. Performing the angular integration yields the result

$$F_{ks,\omega}^{(\lambda\nu)}(\Omega) = \frac{1}{2\pi v_F k} \int_{q_-}^{q_+} q dq \left| M_{q\Omega}^{(\lambda)} \right|^2 \left(\frac{q_+^2 - q^2}{q^2 - q_-^2} \right)^{s'/2}, \quad (12)$$

$$q_{\pm} = \left| \frac{|\mu + \omega + \nu\Omega|}{v_F} \pm k \right|,$$

where $s' \equiv s \operatorname{sgn}(\mu + \omega + \nu\Omega)$.

For a discussion of the lifetime, we now consider the on-shell case, $\omega = \epsilon_{\mathbf{k}s}$. For the Rayleigh mode with $c_R \ll v_F$, we find $s' = +$, $q_+ \simeq 2k$ and $q_- = 0$, yielding for both $\nu = \pm$ the analytical result

$$F_k^{(R)}(\Omega) = \frac{C}{2\pi} \frac{\Omega^2 \sqrt{1 - (\Omega/2c_R k)^2}}{\rho_M v_F c_l^4} \Theta(2kc_R - \Omega) \quad (13)$$

with the Heaviside function Θ . The Eliashberg functions for the other two phonon modes have to be computed numerically. Together with Eq. (13) they are shown in Fig. 1. Numerically, after a rescaling we find almost *universal* behavior in the sense that the functions $(k_F/k)^2 F_{ks}^{(\lambda\nu)}(k\Omega/k_F)$ are essentially independent of k . The $\Omega \rightarrow 0$ behavior is dominated by the Rayleigh mode with $F(\Omega) \sim \Omega^2$, but at higher energy scales (in particular outside the regime shown in Fig. 1), the two other modes are much more important.

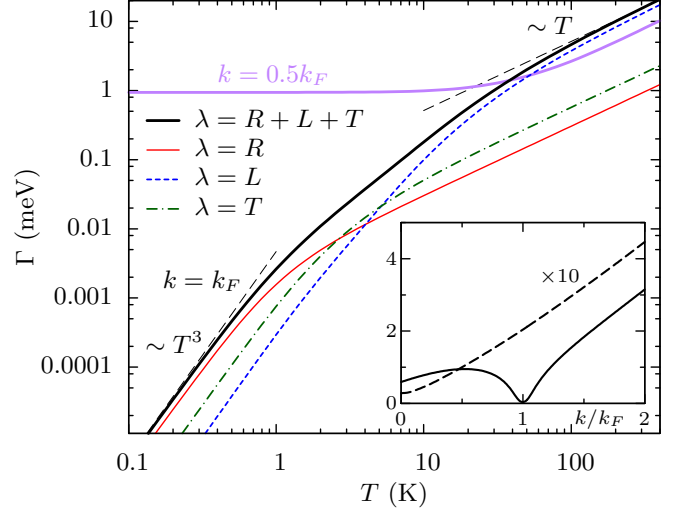


FIG. 2. (Color online) Main panel: T -dependence of the decay rate Γ for $k = k_F$ and for $k = 0.5k_F$. For $k = 0.5k_F$, only the L mode gives significant contributions. Inset: k -dependence of Γ for $T = 3.9$ K (solid line) and for $T = 392$ K (dashed line; the shown result has to be multiplied by 10).

The resulting quasi-particle decay rate $\Gamma_k(T)$ then follows from Eq. (10) and is shown in Fig. 2. The decay rate is dominated by the L mode except for very low energy scales, i.e., when the particle is near the Fermi surface, $k \approx k_F$, and temperature is low, $T \lesssim T_{BG}$. For high temperatures, however, Eq. (10) predicts a characteristic $\Gamma \sim T$ law, which allows to identify electron-phonon scattering processes in practice. For $k = k_F$ and $T \ll T_{BG}$, the decay rate is dominated by the R mode, and we obtain

$$\Gamma_{k_F}(T) = \frac{28\zeta(3)C}{\pi} \frac{\alpha^2 c_R^3 k_F^3}{\rho_M v_F c_l^4} \left(\frac{T}{T_{BG}} \right)^3 \quad (14)$$

with $\zeta(3) \simeq 1.202$ [26]. This T^3 law and the crossover to the linear T dependence for $T \gg T_{BG}$ are shown in Fig. 2. We note that away from the Fermi surface, the $T = 0$ decay rate stays finite and scales as $\Gamma_k \sim |k - k_F|^3$ for $k \rightarrow k_F$.

Resistivity.— Next we compute the phonon contribution to the resistivity, ρ , using a quasiclassical Boltzmann transport theory as employed recently for graphene [14, 15],

$$\rho = \frac{2}{e^2 v_F^2 D(\mu)} \frac{1}{\langle \tau \rangle}, \quad \langle \tau \rangle = \frac{\int d\epsilon (-\partial_\epsilon n_F) D(\mu + \epsilon) \tau(\epsilon)}{\int d\epsilon (-\partial_\epsilon n_F) D(\mu + \epsilon)}, \quad (15)$$

with the density of states $D(E) = |E|/(2\pi v_F^2)$. This approach is valid for $|\mu| \langle \tau \rangle \gg 1$, which is equivalent to $G_Q \rho \ll 1$ with the conductance quantum $G_Q = e^2/h$. The inverse of the energy-dependent electron-phonon transport scattering time $\tau(\epsilon_{\mathbf{k}s})$ follows from Fermi's golden rule as a sum over independent phonon mode (λ) contributions. The result can again be expressed

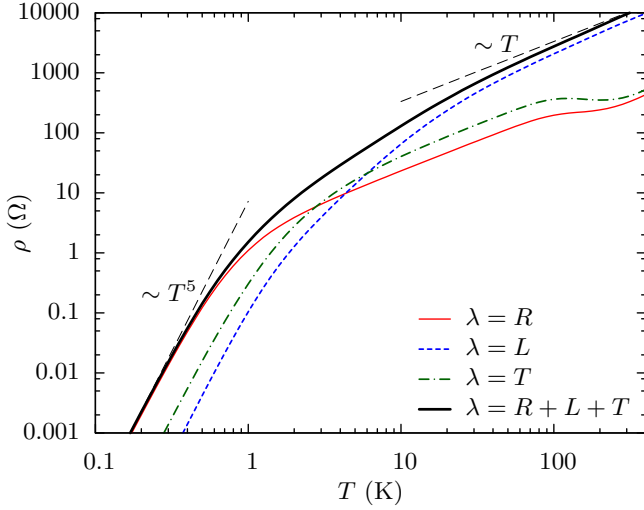


FIG. 3. (Color online) Temperature dependence of the phonon contribution to the surface resistivity. Note the double-logarithmic scales. Individual contributions of each phonon mode are also shown.

using a “transport” Eliashberg function $\mathcal{F}_{\mathbf{k}s}^{(\lambda\pm)}(\Omega)$ given by Eq. (11) with $\omega = \epsilon_{\mathbf{k}s}$ and an additional factor $(1 - \cos \theta_{\mathbf{k},\mathbf{q}})$ in the integral, where $\theta_{\mathbf{k},\mathbf{q}} = \theta_{\mathbf{k}+\mathbf{q}} - \theta_{\mathbf{k}}$ is the angle between \mathbf{k} and $\mathbf{k} + \mathbf{q}$. After the angular integration, we obtain \mathcal{F} as in Eq. (12) but with an additional factor $(q^2 - q_-^2)/[2k(q_+ - k)]$ in the integrand. The resulting functions are depicted in the inset of Fig. 1.

After some algebra, we arrive at [27]

$$\frac{1}{\tau(\epsilon_{\mathbf{k}s})} = \sum_{\lambda,\nu=\pm} \alpha^2 \int_0^\infty d\Omega \mathcal{F}_{\mathbf{k}s}^{(\lambda,\nu)}(\Omega) \quad (16)$$

$$\times \nu n_B(\nu\Omega) \frac{1 - n_F(\epsilon_{\mathbf{k}s} + \nu\Omega)}{1 - n_F(\epsilon_{\mathbf{k}s})}.$$

In Fig. 3, we show the full T dependence of the phonon-induced resistivity ρ . For $T \ll T_{\text{BG}}$, the resistivity is dominated by the $\Omega \rightarrow 0$ behavior of $\mathcal{F}(\Omega)$. The latter comes from the R mode with $\mathcal{F} \sim \Omega^4$, which implies $\rho \sim T^5$ as $T \rightarrow 0$. The prefactor can be evaluated exactly,

$$G_Q \rho(T \rightarrow 0) = \frac{1488\zeta(5)C}{\pi} \frac{\alpha^2 c_R^3 k_F^2}{\rho_M v_F^2 c_l^4} \left(\frac{T}{T_{\text{BG}}} \right)^5, \quad (17)$$

where $\zeta(5) \simeq 1.037$ [26]. We thus recover the standard BG power law, $\rho \sim T^5$, as in bulk 3D metals [28] which is here caused by the coupling to the Rayleigh surface phonon mode. For $T \gg T_{\text{BG}}$, on the other hand, we find a $\rho \sim T$ law predominantly due to the L mode. For $T \approx T_{\text{BG}}$, all three phonon modes are important.

Conclusions.— We have formulated an analytically tractable effective low-energy theory of the surface Dirac fermion state in a strong TI with deformation-potential coupling to acoustic phonons. The influence of phonons could be observed as characteristic temperature-dependent decay rate Γ of quasi-particles in ARPES, or from their T -dependent contribution to the surface resistivity. The phonon-mediated effective interaction among surface fermions can also be attractive at low frequencies, possibly allowing for superconducting correlations; however, this topic as well as studies of the electron-induced modification of phonon properties in this system or the physics near the Dirac point ($k_F = 0$) are left for future work. We hope that our predictions will soon be tested experimentally.

This work was supported by the Humboldt foundation and by the SFB TR 12 of the DFG.

-
- [1] M.Z. Hasan and C.L. Kane, Rev. Mod. Phys. **82**, 3045 (2010).
 - [2] X.L. Qi and S.C. Zhang, arXiv:1008.2026.
 - [3] L. Fu and C.L. Kane, Phys. Rev. B **76**, 045302 (2007).
 - [4] X.L. Qi, T.L. Hughes, and S.C. Zhang, Phys. Rev. B **78**, 195424 (2008).
 - [5] D. Hsieh *et al.*, Nature **460**, 1101 (2009); Y. Chen *et al.*, Science **329**, 659 (2010); L.A. Wray *et al.*, Nat. Phys. **6**, 855 (2010).
 - [6] N.P. Butch *et al.*, Phys. Rev. B **81**, 241301(R) (2010).
 - [7] D.X. Qu, Y.S. Hor, J. Xiong, R.J. Cava, and N.P. Ong, Science **329**, 821 (2010).
 - [8] J.G. Analytis *et al.*, Nat. Phys. **6**, 960 (2010).
 - [9] W. Richter, H. Köhler, and C.R. Becker, phys. stat. sol. (b) **84**, 619 (1977).
 - [10] J.O. Jenkins, J.A. Rayne, and R.W. Ure, Jr., Phys. Rev. B **5**, 3171 (1972).
 - [11] B.L. Huang and M. Kaviani, Phys. Rev. B **77**, 125209 (2008).
 - [12] K.M.F. Shahil, M.Z. Hossain, D. Teweldebrhan, and A.A. Balandin, Appl. Phys. Lett. **96**, 153103 (2010); J. Qi *et al.*, *ibid.* **97**, 182102 (2010).
 - [13] Ph. Hofmann, Prog. Surf. Sci. **81**, 191 (2006).
 - [14] E.H. Hwang and S. Das Sarma, Phys. Rev. B **77**, 115449 (2008).
 - [15] E. Mariani and F. von Oppen, Phys. Rev. B **82**, 195403 (2010).
 - [16] D.K. Efetov and P. Kim, Phys. Rev. Lett. **105**, 256805 (2010).
 - [17] A. Knäbchen, Phys. Rev. B **55**, 6701 (1997).
 - [18] B. Hellsing, A. Eiguen, and E.V. Chulkov, J. Phys. Cond. Matt. **14**, 5959 (2002).

- [19] P.M. Echenique *et al.*, Surf. Sci. Rep. **52**, 219 (2004).
- [20] S.R. Park *et al.*, Phys. Rev. B **81**, 041405(R) (2010).
- [21] L.D. Landau and E.M. Lifshitz, *Elasticity Theory*, ch. 24 (Pergamon, New York, 1986).
- [22] Y.M. Sirenko, K.W. Kim, and M.A. Stroscio, Phys. Rev. B **56**, 15770 (1997).
- [23] For a phenomenological discussion of a different electron-phonon coupling mechanism in the context of surface acoustic waves, see P. Thalmeier, arXiv:1101.5572.
- [24] C.X. Liu *et al.*, Phys. Rev. B **82**, 045122 (2010).
- [25] H. Zhang *et al.*, Nat. Phys. **5**, 438 (2009).
- [26] M. Abramowitz and I.A. Stegun, *Handbook of Mathematical Functions* (Dover, New York, 1971).
- [27] Equation (16) ignores screening by the surface charge carriers themselves. Note that this approximation is consistent with experimental results in graphene [16].
- [28] N.W. Ashcroft and N.D. Mermin, *Solid State Physics* (Saunders College, Philadelphia, 1976).